CrossMark

Surface tension and density data for Fe–Cr–Mo, Fe–Cr–Ni, and Fe–Cr–Mn–Ni steels

Tobias Dubberstein[1] · Hans-Peter Heller[1] · Jens Klostermann[2] · Rüdiger Schwarze[2] · Jürgen Brillo[3]

Abstract The temperature dependence of surface tension and density for Fe–Cr–Mo (AISI 4142), Fe–Cr–Ni (AISI 304), and Fe–Cr–Mn–Ni TRIP/TWIP high-manganese (16 wt% Cr, 7 wt% Mn, and 3–9 wt% Ni) liquid alloys are investigated using the conventional maximum bubble pressure (MBP) and sessile drop (SD) methods. In addition, the surface tension of liquid steel is measured using the oscillating droplet method on electromagnetically levitated (EML) liquid droplets at the German Aerospace Centre (DLR, Cologne). The data of thermophysical properties for Fe–Cr–Mn–Ni is of major importance for modeling of infiltration and gas atomization processes in the prototyping of a "TRIP-Matrix-Composite." The surface tension of TRIP/TWIP steel increased with an increase in temperature in MBP as well as in SD measurement. The manganese evaporation with the conventional measurement methods is not significantly high within the experiments ($\Delta_{Mn} < 0.5$ %). The temperature coefficient of surface tension ($d\sigma/dT$) is positive for liquid steel samples, which can be explained by the concentration of surface active elements. A slight influence of nickel on the surface tension of Fe–Cr–Mn–Ni steel was experimentally observed where σ is decreased with increasing nickel content. EML measurement of high-manganese steel, however, is limited to the undercooling state of the liquid steel. The manganese evaporation strongly increased in excess of the liquidus temperature in levitation measurements and a mass loss of droplet of 5 % was observed.

✉ Tobias Dubberstein
dubberst@iest.tu-freiberg.de

Hans-Peter Heller
heller@iest.tu-freiberg.de

Jens Klostermann
jens.klostermann@imfd.tu-freiberg.de

Rüdiger Schwarze
ruediger.schwarze@imfd.tu-freiberg.de

Jürgen Brillo
juergen.brillo@dlr.de

[1] Institute of Iron and Steel Technology, Tu Bergakademie Freiberg, Leipziger Straße 34, 09599 Freiberg, Germany

[2] Institute of Mechanics and Fluid Dynamics, Tu Bergakademie Freiberg, Lampadiusstraße 4, 09599 Freiberg, Germany

[3] Institut für Materialphysik im Weltraum, Deutsches Zentrum für Luft- und Raumfahrt (DLR), 51170 Cologne, Germany

Introduction

High-manganese steels exhibit excellent mechanical and material properties [1, 2]. Recently, developed members of this class are based on Fe–Mn–C with manganese content up to 30 wt% and Fe–Cr–Mn–Ni as-cast steel with manganese content up to 7 wt% [3, 4].

In order to precisely model the casting processes and mold filling, i.e., infiltration of liquid steel into open foam ceramics for a "TRIP-Matrix-Composite" with superior mechanical properties, the fluid flow and the metal jet disintegration of Fe–Cr–Mn–Ni steel in vacuum inert gas atomization, thermophysical properties (surface tension, density, and viscosity) of the melt need to be measured [4–6]. For instance, Buchwalder et al. [7] investigated the weldability of high alloyed Fe–Cr–Mn–Ni steels. They pointed out the necessity of the accurate knowledge of material properties in the liquid state to describe and model welding phenomena.

For manganese- and chromium-based steel alloys, the precise experimental determination of the surface tension is

by no means straightforward. The main challenge to be mastered is associated with the increased chemical reactivity of Mn and Cr. Chemical reactions of the liquid sample with its crucible may lead to the formation of oxide species at the surface [8]. As these are energetically stable, they lower the overall surface energy. In fact, the presence of dissolved oxygen at the surface of a liquid metal can severely distort the results of the measurements. Only a few ppm of oxygen are sufficient in order to decrease the surface tension by more than 30 %. A similar role is played by sulfur [9, 10]. Both elements can act together, leading partially to a mutual compensation of their negative effects.

Containerless processing techniques can be used in order to suppress reactions of the sample with the crucible. This has been demonstrated in a large number of cases [11–13]. Only the atmosphere can contribute as a possible source of oxygen in containerless processing.

However, manganese can also lead to an increased evaporation of sample material at a high temperature. For instance, the partial vapor pressure of Mn in a Fe–Cr–Mn–Ni alloy at 1600 °C, which is two orders of magnitude larger than the partial vapor pressure of chromium. It is even three orders of magnitude larger than for iron [8]. In general, the mass loss that is encountered during evaporation is determined by three factors: the partial vapor pressure of an element, its transport to the surface, and the ratio of the surface area to the bulk volume [14].

Hence, for Mn-containing materials the application of containerless techniques, such as electromagnetic levitation (EML), is also complicated. Generally, the ratio of the free liquid surface to the bulk volume is larger for levitating droplet compared to a liquid sample processed in a container. Moreover, due to electromagnetic stirring, the amount of evaporating material being transported to the surface is significantly increased.

The maximum bubble pressure (MBP) technique could eventually provide an alternative [15]. With this method, surface tension and density are measured via the maximum gas pressure needed in order to create and detach a bubble in the melt. As a clean surface is created once again for each bubble, this method should probably be less sensitive to evaporation and oxidation of the sample material than sessile drop (SD) and EML.

It is the main goal of the present work to provide surface tension data of laboratory Fe–Cr–Mn–Ni steels as functions of temperature. AISI 304 and AISI 4142 is used to compare all methods with a standard steel in a high alloyed and a low alloyed state. To do this, surface tension is measured using three different methods: classical container-based SD method, classical semicontainer-based MBP method, and the containerless technique of EML. From analytical comparisons of the results obtained from each method, the aim is to identify useful surface tension data for high-manganese Fe–Cr–Mn–Ni alloy.

Materials and methods

The wrought steels are manufactured using a vacuum induction melting furnace under a protecting inert gas atmosphere of Ar 5.0 (<2 ppm O_2). The chemical compositions of the as-cast steels are analyzed by means of optical emission spectrometry (OES). Carbon and sulfur content is determined using a combustion technique (LECO CS-244), and the total oxygen and nitrogen contents are obtained after sample casting by hot gas extraction (BRUKER G8 GALILEO ON/H). The chemical compositions of the alloys AISI 304, AISI 4142, and Fe–Cr–Mn–Ni (16–7–3 and 16–7–9) are presented in Table 1. The liquidus temperature of alloys is calculated by FactSage 6.3.1 using SGSL database.

Maximum bubble pressure method

The setup of the used MBP apparatus is schematically shown in Fig. 1. The apparatus consists of a high-frequency induction furnace ($P = 5$ kW, $f = 300$ kHz), a sharp-edged yttrium partially stabilized zirconia Y-PSZ capillary (ID = 1.177×10^{-3} m, length = 0.4 m) with a wall thickness at the tip of the capillary of <30 μm, and a piezo resistive pressure sensor.

Table 1 Main chemical composition of investigated as-cast steel alloys before experimental trials

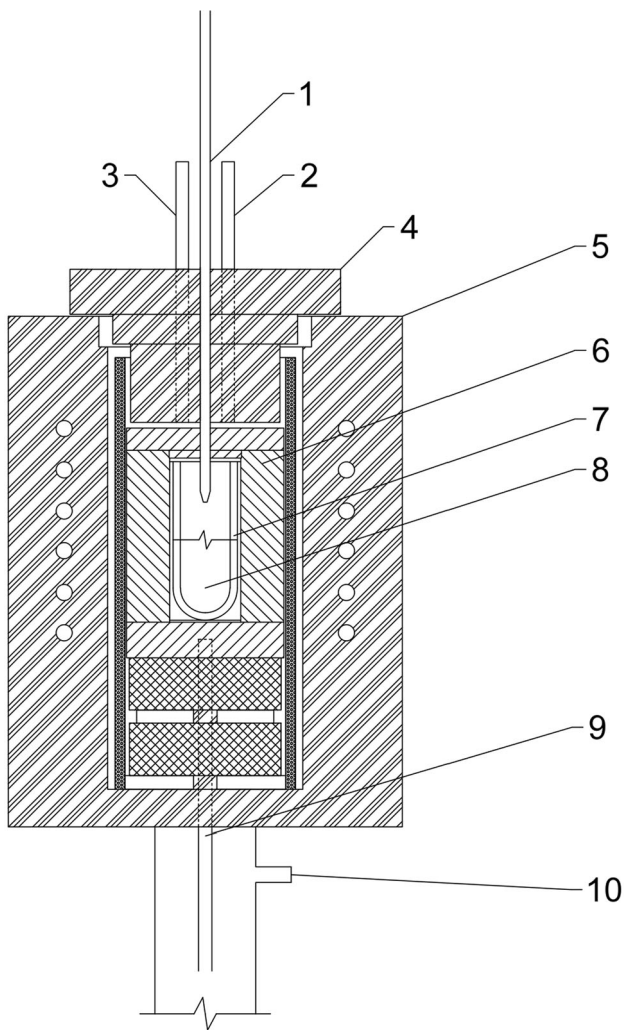| Sample	Fe + others (wt%)	C	Si	Mn	Cr	Ni	Al	Mo	Ti	N (ppm)	$O^{aa}_{tot.}$	S	P	$T_{liq.}$ (°C)
AISI 304	Bal	0.016	0.46	1.38	18.3	9.16	0.0025	0.34	0.0018	443	55	125	289	1440
AISI 4142	Bal.	0.422	0.26	0.85	1.1	0.21	0.0106	0.18	0.0019	40	80	267	200	1490
16–7–3	Bal.	0.027	0.88	7.19	15.9	2.95	0.0010	0.09	<0.001	154	30	77	166	1442
16–7–9	Bal.	0.035	0.95	7.12	15.9	9.20	0.0033	0.11	<0.001	226	14	70	176	1397

[a] Total oxygen content

Fig. 1 Experimental apparatus using the maximum bubble pressure method (*1* Y-PSZ capillary, *2* differential pressure measurement, *3* top argon, *4* upper shell, *5* furnace with high-frequency inductor, *6* graphite crucible, *7* dense alumina crucible ($Al_2O_3 \geq 99.5$ vol%), *8* liquid melt, *9* type-B thermocouple (Pt30Rh-Pt6Rh), *10* bottom argon)

In order to perform the experiment, Ar (5.0) gas is flushed through the furnace ($\approx 2 \times 10^{-3}$ Nm^3 s^{-1}) from the top and the bottom in order to minimize the amount of oxygen in the vicinity of the sample. The liquid alloys are contained in an alumina crucible with an inner diameter of 26 and 75 mm in length. To ensure the precise determination of the pressure maximum at the moment of the bubble detachment, the ratio of the system to the bubble volume (V_s/V_b) should exceed 2.000 [16]. This is assured in the current work ($V_s/V_b > 15.000$). Hence, no undesired hydrodynamic effects, like the occurrence of bubble series, are observed.

The MBP is measured in an immersion depth from 10 to 20 mm from the liquid metal surface. It is ensured that the

ratio (r/a) of the capillary radius r to the capillary constant a is <0.7, where a is defined as followed:

$$a^2 = \frac{2\sigma}{g\left(\rho - \rho_{argon}\right)} \tag{1}$$

In (1), σ is the surface tension, g the gravitational acceleration, ρ the mass density of the fluid, and ρ_{argon} is the density of the argon gas at the temperature of 15 °C.

Hence, the boundary condition of the by Schrödinger corrected Cantor equation to calculate the surface tension using the bubble pressure and the immersion depth of the capillary is fulfilled [17, 18]:

$$\sigma = \frac{rp}{2}\left(1 - \frac{2}{3}\left(\frac{r\rho g}{p}\right) - \frac{1}{6}\left(\frac{r\rho g}{p}\right)^2\right) \tag{2}$$
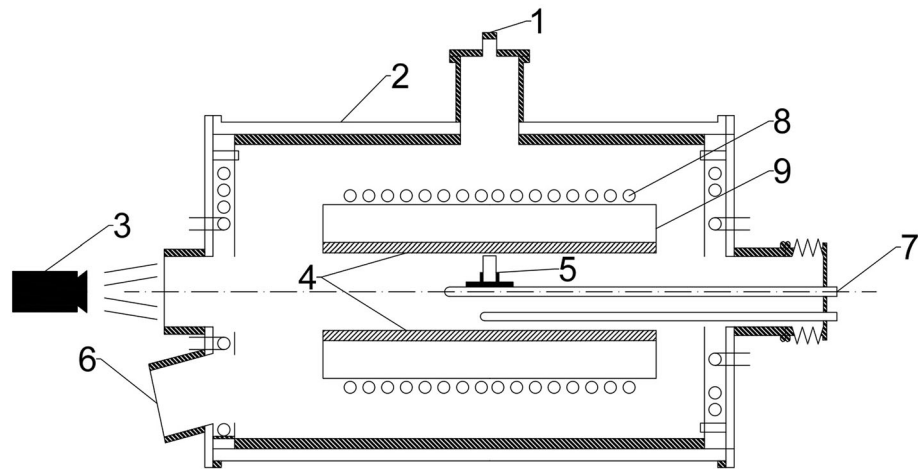
$$p = p_{max} - \rho gh \tag{3}$$

In Eqs. (2) and (3), r is the inner capillary radius, h the immersion depth of the capillary, and p_{max} is the maximum bubble pressure. The density is derived from the slope of the linear fit of the MBP and the immersion depth of capillary.

Sessile drop

A scheme of the SD method is presented in Fig. 2. The main setup is located inside a vacuum chamber. In order to remove impurities from the ambient gasses, it is evacuated ≤0.1 mbar. For the experiment, the vacuum vessel is flushed with argon (5.0). The sample is heated inside a graphite susceptor having the shape of a tube. The susceptor is heated inductively using an RF of 10 kW and 100 kHz. The sample is placed into the furnace using a precise linear guiding. A high-temperature zirconia oxygen probe is installed for the analysis of the oxygen partial pressure p(O$_2$) in the gas outlet stream of the vessel at a cell reference temperature of about 750 °C. The sample temperature is controlled via a type-B thermocouple (Pt30Rh–Pt6Rh) and the furnace temperature is adjusted by Eurotherm 2408 PID controller. An alumina crucible (ID = 8 mm) is used as sample container and substrate in order to generate a large asymmetric droplet profile [19–22].

The drop profile is varied using different sample masses. The best fit of drop mass of the recorded drop shape and the calculated shape numerical solving the Young–Laplace equation is set for the SD experiments. A CCD-camera (resolution 640 × 480 pixels) constantly recorded the drop profile [23].

Fig. 2 Experimental apparatus using the sessile drop method (*1* argon inlet, *2* stainless steel vessel, *3* CCD-camera, *4* graphite tube, *5* sample, *6* high-temperature zirconia oxygen probe, *7* linear guiding with thermocouple type-B, *8* RF-furnace, *9* alumina tube)

In the case of the MBP and the SD experiments, the argon gas is provided by a liquid gas tank ($V = 3.4$ m^3, $p = 32$ bar) with a vaporizer unit. The inert gas is transported from the gas supply throughout the experimental furnaces using polished stainless steel ring line tubes with very low gas leakage rate. The oxygen partial pressure of argon gas is approximately 7×10^{-7} bar and therefore below the customer specification of 2 ppm O$_2$ and was determined using a high-temperature oxygen sensor before the experimental trials. In order to obtain material properties relevant for metallurgical processes, namely casting and metal spraying, no further gas purification is installed. No oxygen increase by any possible H$_2$O dissociation reaction in the furnace atmosphere is recorded within the experimental trials in high-temperature SD experiments. All crucible containers are annealed in argon atmosphere for purification and stored within a dehydrator before experimental trials.

In sessile drop, the argon flow is directed on the graphite tube in the vessel and the oxygen impurity in gas can react with carbon forming carbon monoxide. Considering the supplier specification, the oxygen impurity in argon is max. 2E−06 bar. For the CO reaction, the equilibrium constant K is considered as:

$$K = \frac{[a_C] \cdot [a_O]}{pCO} \tag{4}$$

And the equilibrium constant is 2.30E−3 at 1600 °C and the following partial pressure of CO, CO$_2$, and pO$_2$ and the oxygen activity were calculated (Table 2) [24] S.18. The measured oxygen partial pressure at the gas outlet in SD experiments was of the magnitude of 10^{-17} bar. In all cases, the oxygen partial pressure inside the furnace is too low for any significant increase in oxygen activity of samples.

Electromagnetic levitation

EML experiments are performed in a standard stainless steel high vacuum chamber which has been described in detail in [11, 12, 25]. The chamber is filled with 800 mbar Ar (6.0) after prior evacuation to approximately 10^{-7} mbar. Before an experiment, the samples (typical diameter of 4 mm) are placed in the center of a levitation coil, to which a high-frequency inhomogeneous electro-magnetic field is applied. The eddy currents induced by the fields in the metal sample generate together with the fields a Lorentz force which stably positions the sample against gravity. Due to ohmic losses of the eddy currents inside the sample, it is heated and molten. In order to adjust a certain desired temperature, the sample is cooled in a laminar flow of helium gas.

The temperature is measured by a pyrometer focussed at the sample from the side. As the emissivity was generally not known, it was determined from the pyrometer output signal at the known liquidus temperature T_L under the valid assumption that, within the operating wavelength range of the pyrometer, the emissivity of the specimen material does not change with temperature. The details of this procedure are described in [26]. In the present work, values for T_L are obtained from FactSage 6.3.1 calculations, see Table 1.

The frequencies of the droplet oscillations serve as a direct measure of the surface tension σ. Generally, a spectrum of five different frequencies, ω_m, from the oscillating droplet is observed. These frequencies are numbered by m with $m = -2, -1, 0, 1, 2$. They are measured by recording 5000 images of the oscillating drop using a C-MOS camera with 400 frames per second (fps). An edge detection and analysis algorithm produces frequency spectra from the time signals, such as the one shown in Fig. 3.
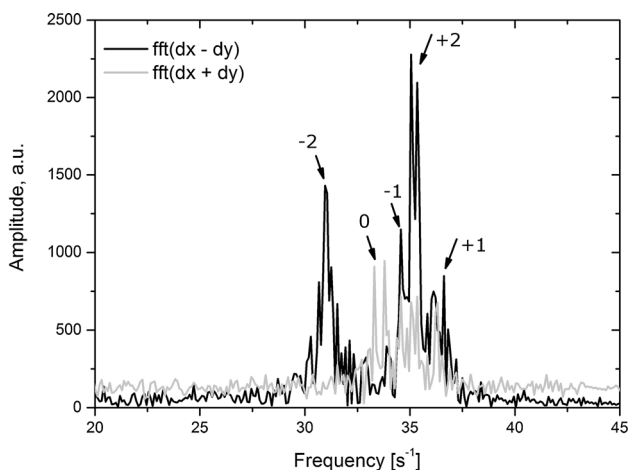
Fig. 3 Spectrum of liquid Fe–Cr–Ni droplet in levitation experiment at 1510 °C
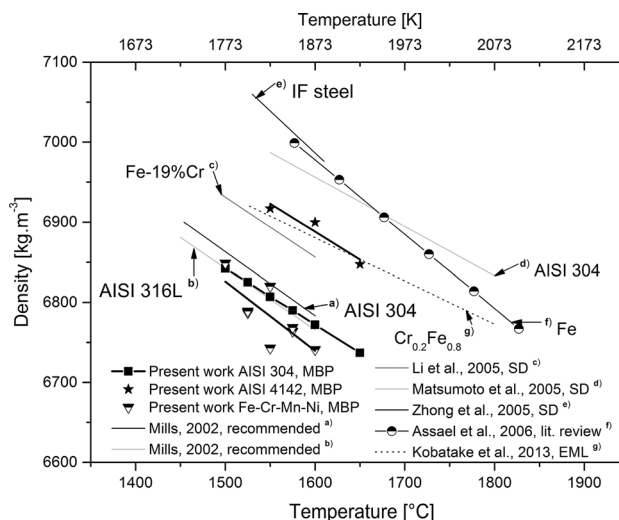

Fig. 4 Density data for AISI 304, AISI 4142, and Fe–Cr–Mn–Ni presented with the data of Mills [32], Li et al. [30], Matsumoto et al. [33], Zhong et al. [29], Assael et al. [31], and Kobatake et al. [34]

They are Fourier transforms of the difference and the sum signal of two perpendicular radii. Using symmetry rules, the frequencies ω_m, marked by arrows in Fig. 3, can be identified.

σ is calculated from these frequencies using the sum rule of Cummings and Blackburn [27]:

$$\sigma = \frac{3M}{160\pi}\sum_{m=-2}^{2}\omega_m^2 - 1.9\Omega^2 - 0.3\left(\frac{g}{a}\right)^2\Omega^{-2} \qquad (5)$$

Here, M is the mass of the sample, a its radius, and g is the gravitational acceleration. In Eq. (5), the parameter Ω corrects for the magnetic pressure. It is calculated from the three translational frequencies, ω_X, ω_Y, and ω_Z corresponding to the horizontal and vertical movements of the center of gravity of the sample:

$$\Omega^2 = 1/3\left(\omega_X^2 + \omega_Y^2 + \omega_Z^2\right) \qquad (6)$$

From measurements published in [28], the relative error $\Delta\sigma/\sigma$ is estimated to be about 5 %.

Results

Density

Figure 4 shows the density data of liquid AISI 304, AISI 4142, and Fe–Cr–Mn–Ni alloys as function of temperature measured by the MBP technique (Table 2). When a temperature ranges from 1500 to 1650 °C, ρ accepts values from 6.74×10^3 to 6.84×10^3 kg m^{-3} for AISI 304, and for AISI 4142, when another temperature ranges from 1550 to 1650 °C, ρ admits values from 6.91×10^3 to 6.85×10^3 kg m^{-3}. For Fe–Cr–Mn–Ni alloys in the range of 3–9 wt% Ni content, no significant influence of nickel on density is measured. Density decreases from

Table 2 Calculated values for CO, CO$_2$ equilibrium

pCO	4.00E−06 bar
pCO$_2$	7.86E−16 bar
pO$_2$	7.15E−27 bar
a[O]	2.49E−10 %

6.83×10^3 kg m^{-3} at 1500 °C to 6.74×10^3 kg m^{-3} at 1600 °C.

For all investigated alloys, ρ decreases linearly with temperature. The following linear relation can be adjusted to the data:

$$\rho(T) = \rho_{\text{ref}} + \rho_{\text{T}}(T - T_{\text{ref}}) \qquad (7)$$

where ρ_{ref} is the density at reference temperature T_{ref} and $\rho_{\text{T}} = \partial\rho/\partial T$ the corresponding temperature coefficient. The results, that is, the parameters ρ_{ref} and ρ_{T}, are listed in Table 3 for the three alloys.

The experimental values for a high alloyed austenitic stainless steel (AISI 304) are below the values of a low alloyed interstitial-free (IF) steel of Zhong et al. [29] and coincide well with the literature findings between low and high alloyed iron alloys.

The density measured for AISI 4142 is larger than for AISI 304 and Fe–Cr–Mn–Ni. This is explained by the significant decrease of the mass density with an increase in the chromium content in the stainless steel matrix. This is also evident in the data presented by Li et al. [30].

Figure 4 also shows the density of pure liquid iron recommended by Assael et al. [31]. This demonstrates that there is good agreement with the data of the low alloyed IF steel from Zhong et al. [29].

Table 3 Linear correlation of density for AISI 304, AISI 4142, and Fe–Cr-Mn-Ni based on MBP results

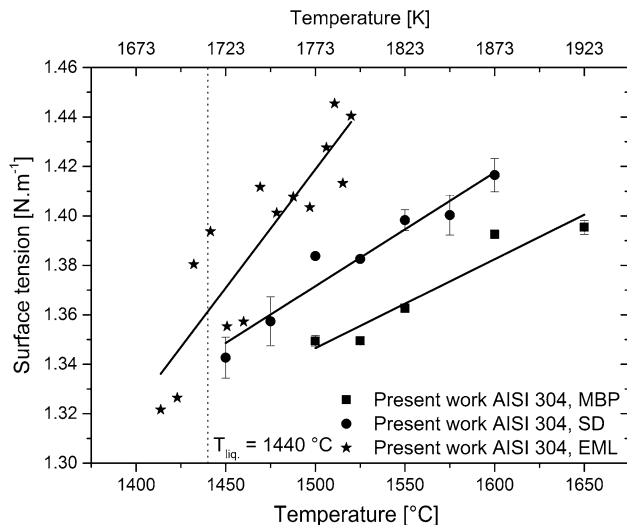| Sample	T_{ref} (°C)	ρ_{ref} (10^3 kg m^{-3})	ρ_T (kg m^{-3} K^{-1})	ΔT (°C)
AISI 304	1500	6.84	−0.70	1500–1650
AISI 4142	1550	6.92	−0.69	1550–1650
Fe–Cr–Mn–Ni	1500	6.83	−0.86	1500–1600

Fig. 5 Results of the surface tension measurements for AISI 304 steel

Surface tension

Fe–Cr–Ni (AISI 304)

In Fig. 5, the results are presented for surface tension measurements of the as-cast AISI 304 steel. One data point of the bubble pressure results is the average of at least three independent measurements at constant temperature. For MBP, SD, and EML values, the temperature coefficient of the surface tension is positive and is in the order of 10^{-4} N m^{-1} K^{-1}. For MBP, the surface tension increases from 1.35 to 1.40 Nm^{-1} from 1500 °C to 1650 °C. For SD, the surface tension is increasing from 1.34 N m^{-1} (1450 °C) to 1.42 N m^{-1} (1600 °C). However, in the case of the levitation experiments, σ increases strongly from 1.32 N m^{-1} for 1414 °C to 1.44 N m^{-1} for 1520 °C. As it can also be observed in Fig. 5, an undercooling of approximately 50 K of the liquid droplet for AISI 304 in EML is achieved before immediate solidification of the droplet occurred. There is severe scattering in the experimental data for EML at temperatures higher than 1450 °C, which is in the vicinity of the liquidus temperature for Fe–Cr–Ni steel specimens. In all measurement methods, the surface tension data correspond to a linear regression and the fit is plotted as a black line. The scatter of data points in bubble pressure and SD techniques of the present work for

AISI 304 is not significantly higher in comparison to the levitation technique.

Within the manufacture of the as-cast steel samples at the IEST, using induction furnace without any slag work, no calcium content in chemical composition is present in samples melting. Therefore, in the chemical composition of all considered alloys, the analyzed sulfur content (presented in Table 4) is considered as the soluble sulfur content and no CaS formation in specimen is observed. A total oxygen content of 46 ppm $O_{tot.}$ is low in relation to the large aluminum content of 203 ppm Al forming alumina precipitations. Hence, the soluble oxygen content is negligible in the present steel samples and it is assumed to not significantly modifying the surface tension.

Fe–Cr–Mo (AISI 4142)

The results for low alloyed AISI 4142 are displayed in Fig. 6. In bubble pressure results, the surface tension increased from 1.27 N m^{-1} at 1550 °C to 1.29 N m^{-1} at 1650 °C. The levitation results in the upper temperature regime are in the vicinity of the MBP results. Furthermore, in EML, the surface tension steadily increases with the temperature. However, SD results are higher than the MBP and EML findings. In EML, surface tension is increasing from 1.40 N m^{-1} (1500 °C) to 1.46 N m^{-1} (1650 °C). According to the chemical analyses made after the experiments, no contamination by a crucible dissociation is observed in the samples of the conventional measurement methods. The oxygen content in samples of SD and MBP is not increasing by the orders of magnitude as reported for AISI 430 [35]. However, the sulfur content in SD experiments after the experiments is below the initial sulfur content in analysis, as presented in Table 1.

In all investigated Fe–Cr–Mo and Fe–Cr–Ni samples, there is a significant sulfur drop after the experiments using the SD technique (Table 4).

The equations to calculate the surface tension based on the present work for AISI samples are presented in Table 5.

Fe–Cr–Mn–Ni TRIP/TWIP steel

In the case of the MBP and the SD results, the surface tension is increasing linearly together with the augmentation of temperature, Fig. 7. The sulfur content before and after the experiments, like in Table 6, has a dominant

Table 4 Mean chemical composition after experimental trials using MBP, SD and EML

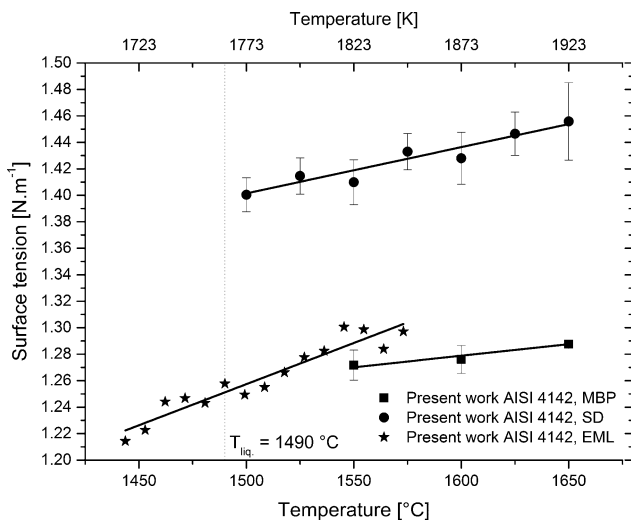| Sample	Method	Fe + others (wt%)	C	Si	Mn	Cr	Ni	Mo	Al	Ti	N (ppm)	O[a]$_{tot.}$	S	P
AISI 304	MBP	Bal.	0.025	0.43	1.32	17.8	9.07	0.35	0.0203	0.004	205	46	141	244
AISI 304	SD	Bal.	0.018	0.48	1.19	18.4	9.01	0.34	0.0010	0.001	99	20	87	298
AISI 304	EML	Bal.	0.016	0.43	0.66	18.3	9.91	0.33	0.0010	0.001	12	21	75	293
AISI 4142	MBP	Bal.	0.429	0.26	0.83	1.08	0.19	0.18	0.0110	0.002	35	14	265	118
AISI 4142	SD	Bal.	0.412	0.28	0.77	0.70	0.18	0.17	0.0202	0.002	15	5	197	192
AISI 4142	EML	–	0.400	–	–	–	–	–	–	–	7	19	245	–

[a] Total oxygen content

Fig. 6 Results of surface tension measurements for AISI 4142 steel

impact on the surface tension. Furthermore, a high manganese content of approximately 7 wt% Mn in Fe–Cr–Mn–Ni alloys is decreasing the surface tension more compared to the results for AISI 304 stainless steel, Fig. 5. This significant influence of the manganese on the surface tension in the investigated alloys is recently reported for the Fe–Mn binary [36]. The measurement of σ using a conventional bubble pressure technique delivered appropriate results. There is no significant decrease of the manganese or the sulfur content after the measurements using conventional techniques (Table 6). In chemical analysis for

sessile drop, the total oxygen and nitrogen content decreased to 9 ppm O_{tot} and 75 ppm N, respectively, via desorption into the pure argon atmosphere of the vessel. The drop in surface tension values from MBP (1.22 N m^{-1} at 1500 °C) to SD (1.18 N m^{-1} at 1500 °C) techniques is not constituted regarding the chemical analysis after experimental trials. The EML results in low-temperature region are not contrary to the measurement results of conventional bubble pressure results. However, in the case of high-temperature region of steel liquidus temperature ($T_{liq.}$), a very strong evaporation occurred during the series of experiments. The mass loss of the levitated droplet of 16–7–3 Fe–Cr–Mn–Ni is approximately 5 % which is almost the reduction of manganese in EML droplet analyzed after trials. A surface temperature in the vicinity or below $T_{liq.}$ decreases the evaporation from the oscillating droplet to a minimum. An undercooling of approximately 150 K is achieved in EML experiments. The recommended fit parameter of 16–7–3 stainless steel using MBP is in Table 7.

A further Fe–Cr–Mn–Ni sample with 9 wt% nickel (16–7–9) is measured using the MBP method to account for the effect of increasing nickel content on surface tension in the high-manganese steel. Only a small decrease of surface tension with an increase in nickel content is observed from 1.27 N m^{-1} (16–7–3) to 1.24 N m^{-1} (16–7–9) at 1600 °C. As reported for Fe–Ni binary alloy, increasing the nickel content in Fe–Ni decreases only slightly the surface tension [37]. To the knowledge of the authors of the present investigation, none of the available

Table 5 Linear fit to calculate surface tension of AISI 304 and AISI 4142

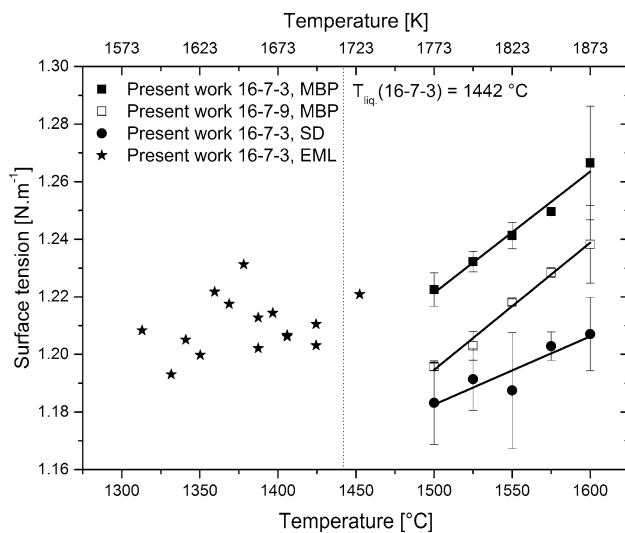| Sample	Method	T_{ref} (°C)	σ_{ref} (N m^{-1})	σ_T (10^{-4} N m^{-1} K^{-1})	ΔT (°C)
AISI 304	MBP	1500	1.35	3.6	1500–1650
AISI 304	SD	1450	1.35	4.6	1450–1600
AISI 304	EML	1415	1.34	9.6	1415–1525
AISI 4142	MBP	1550	1.27	1.7	1550–1650
AISI 4142	SD	1500	1.40	3.5	1500–1650
AISI 4142	EML	1445	1.22	6.2	1445–1575

Fig. 7 Experimental results of the surface tension as a function of temperature for high alloyed Fe–Cr–Mn–Ni as-cast steel using EML, MBP, and SD method

literature is considering the first interaction parameter of nickel on sulfur in Fe–Ni–S ternaries. The temperature coefficient of surface tension for 16–7–3 and 16–7–9 coincides well for MBP results.

Discussion

The primary surface active element, in the present experiment for the steel samples, is sulfur, and hence in agreement with previous findings [6]. According to the Gibbs' adsorption theory, the free surface of a liquid droplet is covered by a monolayer of surface active elements, that is,

sulfur, with lower surface tension than the volume phase. In fact, when the temperature is increasing, sulfur is desorbed into the bulk of the liquid metal as described for sulfur containing Fe–Cr–Ni by McNallan and DebRoy [38] so that the surface tension is augmenting with the rising temperature.

A variation in the steel sulfur content, from low to high sulfur, decreases the surface tension as seen from the data of Brooks et al. [9] for KRA 304 steel (100 ppm S) and Matsumoto et al. [33] AISI 304 steel (250 ppm S) which had a similar mean composition as the AISI 304 of the present work, Fig. 8. A negative slope of the surface tension versus temperature is found by Wunderlich et al. [39] in Fe–C binary with a negligible amount of surface active elements (sulfur). The difference of the data of the present work to the literature for all three independent methods cannot be interpreted in terms of variation in the chemical composition. In the case of the current investigation, sulfur is > 50 ppm in investigated iron alloys and is surface active [40].

The slopes of the linear fit for MBP and SD techniques are in agreement for AISI 304. The difference in the absolute values can be interpreted in terms of the variation in the analyzed sulfur content after the experimental trials. The sulfur is approximately 141 ppm S in MBP and 87 ppm S in SD samples. In SD, the liquid droplet is hold at 1600 °C for 5 min to set a thermal equilibrium in the furnace. In that case, the surface vaporization of sulfur at high temperatures can cause a decrease in the surface adsorption of sulfur, and thus an increase of the surface tension of the sample [41]. In the levitated droplet, the manganese content decreased to approximately 0.66 wt% Mn.

Table 6 Mean chemical composition after experiments for Fe–Cr–Mn–Ni as-cast steel samples

Sample	Method	Fe + others (wt%)	C	Si	Mn	Cr	Ni	Mo	Al	Ti	N (ppm)	O^a_{tot}	S	P
16–7–3	MBP	Bal.	0.042	0.88	7.01	15.7	3.14	0.079	0.0093	0.001	381	15	60	210
16–7–3	SD	Bal.	0.028	0.90	7.02	15.9	2.95	0.054	0.0010	0.001	75	9	50	228
16–7–3	EML	Bal.	0.028	0.96	2.73	16.1	3.14	0.074	0.0042	0.001	14	23	50	228
16–7–9	MBP	Bal.	0.040	1.10	6.98	16.2	8.36	0.094	0.0162	0.001	372	11	60	129

[a] Total oxygen content

Table 7 Summary of the linear fit proposed to calculate the surface tension based on MBP results for high-manganese Fe–Cr–Mn–Ni as-cast steel

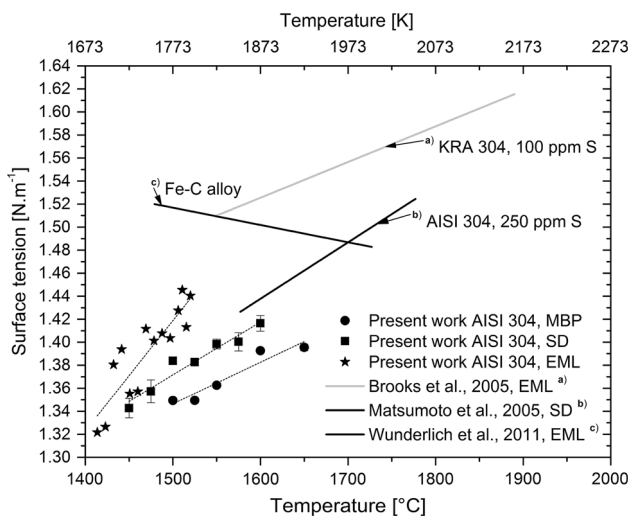| Sample	T_{ref} (°C)	σ_{ref} (N m^{-1})	σ_T (10^{-4} N m^{-1} K^{-1})	ΔT (°C)
16–7–3	1500	1.22	4.2	1500–1600
16–7–9	1500	1.20	4.4	1500–1600

Fig. 8 Results of the surface tension measurements for AISI 304 steel and the literature data of Brooks et al. [9], Matsumoto et al. [33], and Wunderlich et al. [39]

For AISI 4142, the increase of the surface tension in SD, compared to MBP and EML findings, is due to the strong decrease of the surface active sulfur in the liquid droplet after the experiments. There, sulfur decreased from 260 ppm S to approximately 200 ppm S. For MBP and EML analysis sulfur is not significant changed in experiments and the absolute σ values are similar. In MBP, sulfur is increasing throughout all experiments which is the effect of the graphite tube combustion and the mass transfer of sulfur into the liquid sample. Considering that each sample is between 6 and 8 h in a liquid state in MBP, the sulfur increase is not dominant. The Boudouard reaction and a mass transfer of carbon increase the carbon content in the melt [42]. The oxygen activity was not significantly changed in samples after the experiments and is further bound by the aluminum [43].

In the levitation experiments for Fe–Cr–Ni stainless steel (AISI 304) and Fe–Cr–Mn–Ni (16–7–3) as-cast steel,

vaporization from the surface of the oscillating droplet is recorded. For 16–7–3 alloys, vaporization effect is most intensive compared to the AISI 304 levitation samples. For the most part, no evaporation from droplet surface is recorded in the AISI 4142 levitation experiments. Images of recorded droplets are presented in Fig. 9. There is a clear evidence of evaporation from 16–7–3 droplet with initial Mn content of ca. 7 wt%. The mass loss of 5 % results from losing manganese due to the evaporation from the levitated droplet.

A much stronger increase in the surface tension values in comparison to SD and MBP is observed for Cr–Ni stainless steel. The sample mass of EML droplets ($<1.20 \times 10^{-3}$ kg) is sufficient for full chemical analysis. The droplet is pressed to have a flat surface for OES analysis. The sulfur content in the sample is ca. 50 ppm using combustion technique. Quantification of OES analysis in solidified 16–7–3 droplets showed very small manganese content, <3 wt% Mn, the Mn content is significantly changed in oscillating droplet. As reported in the results of an iron–manganese binary, a drop in the manganese content is strongly decreasing the surface tension [36]. In the case of the 16–7–3 droplets, the chemistry changed significantly within the levitation experiment.

Most likely, the higher surface tension in the AISI 304 samples for EML results is the effect of manganese vaporization from droplet surface into vessel atmosphere at elevated temperature as well. Thus, there could be a combined effect of sulfur and manganese evaporation in EML technique for Fe–Cr–Ni stainless steel, which is stronger at high temperature and therefore increasing the temperature coefficient of surface tension to 9.6×10^{-4} N m^{-1} K^{-1} (EML), compared to 4.6×10^{-4} N m^{-1} K^{-1} (SD) and 3.6×10^{-4} N m^{-1} K^{-1} (MBP). In former case, the higher temperature coefficient of surface tension for the oscillation droplet investigation is probably caused by a desorption of surface active elements into the vessel atmosphere.
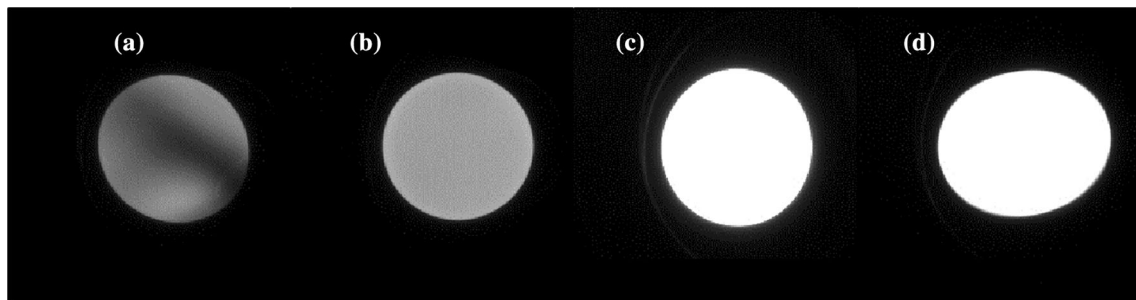

Fig. 9 **a** 16–7–3 droplet with a strong evaporation from surface ($T \gg T_{\text{liq.}}$), **b** 16–7–3 droplet with minor evaporation from surface ($T \ll T_{\text{liq.}}$), **c** Droplet of Fe–Cr–Ni stainless steel at approximately 1500 °C, and **d** low alloyed steel (Fe–Cr–Mo) at $T = 1500$ °C

Summary

In the present work, the oscillating droplet, the sessile drop, and the MBP technique were utilized to measure surface tension of low alloyed AISI 4142, Fe–Cr–Ni stainless steel AISI 304, and high-manganese Fe–Cr–Mn–Ni as-cast steel. The main results are as followed:

1. The temperature coefficient of surface tension is positive for all investigated iron alloys.
2. Sulfur and manganese have major impacts on the surface tension in iron alloys.
3. High-manganese Fe–Cr–Mn–Ni as-cast steel MBP results include a low scattering of data and the surface tension can be measured in high temperatures.
4. The mass loss of solidified droplet after levitation experiment (EML) of 16–7–3 is approximately 5 %, and the chemical analysis after the experiments indicates a significant loss of manganese.
5. The vaporization of manganese is reduced to a minimum in the MBP technique.
6. The chemical stability and the very low aging effects of droplet surfaces in MBP compared to SD and EML propose that data to be used for a simulation of the motion of steel flow in infiltration processes of open foam ceramics and in gas atomization of high-manganese Fe–Cr–Mn–Ni alloys.

References

1. Biermann H, Martin U, Aneziris CG et al (2009) Microstructure and compression strength of novel TRIP-steel/Mg-PSZ composites. Adv Eng Mater 11:1000–1006
2. Aneziris CG, Schärfl W, Biermann H, Martin U (2009) Energy-absorbing TRIP-Steel/Mg-PSZ composite honeycomb structures based on ceramic extrusion at room temperature. Int J Appl Ceram Technol 6:727–735
3. Bouaziz O, Allain S, Scott CP et al (2011) High manganese austenitic twinning induced plasticity steels: a review of the microstructure properties relationships. Curr Opin Solid State Mater Sci 15:141–168
4. Jahn A, Steinhoff K-P, Dubberstein T et al (2013) Phosphor alloyed Cr–Mn–Ni austenitic As-cast stainless steel with TRIP/TWIP effect. Steel Res Int. 85:477–485. doi:10.1002/srin.201300114
5. Klostermann J, Schwarze R, Weider M, Brücker C (2011) Computational fluid dynamic (CFD) simulations of liquid steel infiltration in ceramic foam structures. Part II: application to laboratory-scale experiments. Steel Res Int 82:1113–1121. doi:10.1002/srin.201100093
6. Dubberstein T, Heller H-P (2013) Effect of surface tension on gas atomization of a CrMnNi steel alloy. Steel Res Int 84:845–851. doi:10.1002/srin.201200321
7. Buchwalder A, Rüthrich K, Zenker R, Biermann H (2013) Electron beam welding of high alloy CrMnNi cast steels with TRIP/TWIP effect. Adv Eng Mater 15:566–570
8. Aneziris CG, Jahn A, Weider M, Schärfl W (2010) Refractory materials for casting manganese alloyed. Ref World Forum 2:81–86
9. Brooks RF, Quested PN (2005) The surface tension of steels. J Mater Sci 40:2233–2238. doi:10.1007/s10853-005-1939-2
10. Mills KC, Keene BJ, Brooks RF, Shirali A (1998) Marangoni effects in welding. Philos Trans R Soc A 356:911–925
11. Egry I, Brillo J (2009) Surface tension and density of liquid metallic alloys measured by electromagnetic levitation. J Chem Eng Data 54:2347–2352. doi:10.1021/je900119n
12. Brillo J, Lohofer G, Schmidt-Hohagen F, Schneider S (2006) Thermophysical property measurements of liquid metals by electromagnetic levitation. Int J Mater Prod Technol 26:247–273
13. Brillo J, Egry I (2011) Density of multicomponent melts measured by electromagnetic levitation. Jpn J Appl Phys 50:11RD02. doi:10.1143/JJAP.50.11RD02
14. Shimoji M (1977) Liquid metals : an introduction to the physics and chemistry of metals in the liquid state. Academic Press, New York
15. Dubberstein T, Heller H-P (2013) The thermophysical properties of liquid trip/twip-steel alloys using the maximum bubble pressure method. Adv Eng Mater 15:583–589. doi:10.1002/adem.201200310
16. Fainerman V, Miller R (2004) Maximum bubble pressure tensiometry—an analysis of experimental constraints. Adv Colloid Interface Sci 108–109:287–301. doi:10.1016/j.cis.2003.10.010
17. Lang ND, Kohn W (1971) Theory of metal surfaces: work function. Phys Rev B 3:1215–1223
18. Schrödinger E (1915) Notiz über den Kapillardruck in Gasblasen. Ann Phys 351:413–418. doi:10.1002/andp.19153510306
19. Lee J, Kiyose A, Nakatsuka S et al (2004) Improvements in surface tension measurements of liquid metals having low capillary constants by the constrained drop method. ISIJ Int 44:1793–1799
20. Naidich YV, Eremenko VN (1961) The "large drop" method for determining the surface tension and the density of molten metals. Fiz Met Metallov 11:883–888
21. Padday JF (1972) Sessile drop profiles: corrected methods for surface tension and spreading coefficients. Proc R Soc Lond A 330:561–572. doi:10.2307/78211
22. Tanaka T, Lee J (2014) Experiments. Treatise on Process Metallurgy. Elsevier, Amsterdam, pp 19–34
23. Dubberstein T, Jahn A, Lange M et al (2014) Interfacial reaction between iron-based alloys and polycrystalline Al₂O₃. Steel Res Int 85:1220–1228. doi:10.1002/srin.201300445
24. Oeters F (1989) Metallurgie der Stahlherstellung. Springer, Berlin
25. Egry I, Sauerland S, Jacobs G (1994) Surface tension of levitated liquid noble metals. High Temp High Pressures 26:217–223
26. Egry I, Ratke L, Kolbe M et al (2010) Interfacial properties of immiscible Co–Cu alloys. J Mater Sci 45:1979–1985. doi:10.1007/s10853-009-3890-0
27. Cummings DL, Blackburn DA (1991) Oscillations of magnetically levitated aspherical droplets. J Fluid Mech 224:395–416
28. Mills KC, Brooks RF (1994) Measurements of thermophysical properties in high temperature melts. Mater Sci Eng A 178:77–81
29. Zhong L, Zeze M, Mukai K (2005) Density of liquid if steel containing Ti. ISIJ Int 45:312–315

30. Li Z, Mukai K, Zeze M, Mills KC (2005) Determination of the surface tension of liquid stainless steel. J Mater Sci 40:2191–2195. doi:10.1007/s10853-005-1931-x

31. Assael MJ, Kakosimos K, Banish RM et al (2006) Reference data for the density and viscosity of liquid aluminum and liquid iron. J Phys Chem Ref Data 35:285–300

32. Mills KC (2002) Recommended values of thermophysical properties for selected commercial alloys. Woodhead, Cambridge

33. Matsumoto T, Misono T, Fujii H, Nogi K (2005) Surface tension of molten stainless steels under plasma conditions. J Mater Sci 40:2197–2200. doi:10.1007/s10853-005-1932-9

34. Kobatake H, Brillo J (2013) Density and thermal expansion of Cr–Fe, Fe–Ni, and Cr–Ni binary liquid alloys. J Mater Sci 48:4934–4941. doi:10.1007/s10853-013-7274-0

35. Choe J, Kim HG, Jeon Y et al (2014) Surface tension measurements of 430 stainless steel. ISIJ Int 54:2104–2108. doi:10.2355/isijinternational.54.2104

36. Lee J, Thu Hoai L, Shin M (2011) Density and surface tension of liquid Fe–Mn alloys. Metall Mater Trans B 42:546–549

37. Keene BJ (1988) Review of data for the surface tension of iron and its binary alloys. Int Mater Rev 33:1–37

38. McNallan MJ, DebRoy T (1991) Effect of temperature and composition on surface tension in Fe–Ni–Cr alloys containing sulfur. Metall Mater Trans B 22:557–560

39. Wunderlich RK, Fecht H-J, Schick M, Egry I (2011) Time dependent effects in surface tension measurements of an industrial Fe-alloy. Steel Res Int 82:746–752. doi:10.1002/srin.201000156

40. Sahoo P, Debroy T, McNallan MJ (1988) Surface tension of binary metal-surface active solute systems under conditions relevant to welding metallurgy. Metall Trans B 19:483–491

41. Xue XM, Jiang HG, Sui ZT et al (1996) Influence of phosphorus addition on the surface tension of liquid iron and segregation of phosphorus on the surface of Fe-P alloy. Metall Mater Trans B 27:71–79

42. Dubberstein T, Hötzel M, Hagemann R et al (2011) Some thermophysical properties of liquid Cr–Mn–Ni-Steels. Steel Res Int 82:1122–1128. doi:10.1002/srin.201100096

43. Mills KC, Su YC (2006) Review of surface tension data for metallic elements and alloys: part 1—pure metals. Int Mater Rev 51:329–351. doi:10.1179/174328006X102510